

Available online at [www.synsint.com](http://www.synsint.com)

# Synthesis and Sintering

ISSN 2564-0186 (Print), ISSN 2564-0194 (Online)



Research article

## Role of $Ti_3AlC_2$ MAX phase on characteristics of in-situ synthesized TiAl intermetallics. Part III: microstructure



Maryam Akhlaghi <sup>a</sup>, Esmail Salahi <sup>b,\*</sup>, Seyed Ali Tayebifard <sup>a</sup>, Gert Schmidt <sup>c</sup>

<sup>a</sup> Semiconductors Department, Materials and Energy Research Center (MERC), Karaj, Iran

<sup>b</sup> Ceramics Department, Materials and Energy Research Center (MERC), Karaj, Iran

<sup>c</sup> Faculty of Mechanical, Process and Energy Engineering, TU Bergakademie, Freiberg, Germany

### ABSTRACT

In this paper, the 3<sup>rd</sup> part of a series of publications on the sinterability and characteristics of TiAl– $Ti_3AlC_2$  composites, the microstructure development during the synthesis and sintering processes was studied by scanning electron microscopy (SEM). Chemical evaluation of various phases in the developed microstructures was performed using energy-dispersive X-ray spectroscopy (EDS) in different ways such as point, line scan and two-dimensional elemental map analyses. For this purpose, five samples were fabricated with different percentages of  $Ti_3AlC_2$  MAX phase additive (10, 15, 20, 25, and 30 wt%). Ball-milling and spark plasma sintering (SPS: 900 °C/7 min/40 MPa) of as-purchased Al and Ti powders with already-synthesized  $Ti_3AlC_2$  additive were selected as composite making methodology. SEM/EDS analyses verified the in-situ manufacturing of TiAl/ $Ti_3Al$  intermetallics as the matrix during the SPS process and the presence of  $Ti_3AlC_2$  as the ex-situ added secondary phase. Moreover, the in-situ synthesis of  $Ti_2AlC$ , another member of MAX phases in Ti–Al–C system, was also detected in titanium aluminide grain boundaries and attributed to a chemical reaction between TiC (an impurity in the initial  $Ti_3AlC_2$  additive) and TiAl components.

© 2022 The Authors. Published by Synsint Research Group.

### KEYWORDS

Microstructure  
SPS  
In-situ synthesis  
TiAl– $Ti_3AlC_2$  composites  
SEM/EDS analysis



### 1. Introduction

Titanium aluminides are subjected to broad research works to mature high-temperature industrial applications because of their low density, burn and oxidation resistances, good thermal stability, as well as high strength and Young modulus [1–4]. Anyway, such intermetallics technologically suffer from structural and chemical inhomogeneity, manufacturing difficulty, low ductility at ambient temperature and creep resistance [5–8]. Therefore, microstructural refining is a trick to achieve reproducible and well-balanced mechanical characteristics. For this purpose, several solutions have been proposed such as adding grain growth inhibitors or processing by additive manufacturing (AM) [9, 10] or powder metallurgy (PM) [11, 12] routes. In methods based on

PM, mechanical milling (MM) or double mechanical milling (DMM) of powder mixtures prior to reactive sintering is essential in microstructure refining of synthesized titanium aluminide [13–15]. Spark plasma sintering process (SPS) can be employed to make TiAl materials with refined microstructure [16–19]. The SPS temperature controls the microstructure of titanium aluminides, and as the temperature increases, the microstructure changes [20–23]. Depending on the sintering temperature and the powder composition, various two-phased ( $\gamma+\alpha_2$ ), duplex, and lamellar microstructures were obtained by SPS of pre-alloyed Ti–47Al–2Cr–2Nb [5], Ti–44Al–2Cr–2Nb–1B [5], Ti–48Al–2Cr–2Nb [24], and Ti–46Al–9Nb [25] powders. Similar results were observed for the microstructural compliance of pre-alloyed Ti–43.9Al–4Nb–0.95Mo–0.1B powders with SPS temperature. Duplex,

\* Corresponding author. E-mail address: [e-salahi@merc.ac.ir](mailto:e-salahi@merc.ac.ir) (E. Salahi)

Received 26 December 2021; Received in revised form 19 March 2022; Accepted 19 March 2022.

Peer review under responsibility of Synsint Research Group. This is an open access article under the CC BY license (<https://creativecommons.org/licenses/by/4.0/>).  
<https://doi.org/10.53063/synsint.2022.2182>

fully lamellar, and nearly lamellar microstructures were achieved by SPS of pre-alloyed Ti–43Al–5Nb–2V–1Y powders as a function of the sintering temperature [26]. Anyway, increasing the sintering temperature caused noteworthy growth of the TiAl grains, produced by SPS of Ti–47Al powders, that resulted in drop in hardness and yield strength but slight rise in ductility [27]. Moreover, it was found that achieving a nearly lamellar microstructure results in moderate ductility at room temperature associated with strong creep resistance [28]. An amazing observation was happened during the fabrication of a sample using fine TiAl powders with high amounts of Nb additive, in which increasing the SPS dwell time resulted in microstructural refinement [29].

In recent years, fabrication of composites that are a combination of intermetallics and MAX phases of titanium and aluminum has been considered [30]. It should be noted that the MAX phase materials are relatively a novel class of ternary layered ceramics with burgeoning research potential [31–36]. Mei and Miyamoto [37] sintered TiAl–Ti<sub>2</sub>AlC composites by SPS of Al, Ti and TiC powders. They found that the amount of TiC in the initial powder mixture has a large effect on the microstructure and phase evolution of the sintered composites. Chen et al. [38] manufactured TiAl–Ti<sub>2</sub>AlC composites by hot pressing of a mixture Ti, Al and TiC or C, and found that the nature of the carbon source has a remarkable influence on the resulting microstructures. Yang et al. [39] employed mechanical alloying and SPS for synthesis of TiAl–Ti<sub>2</sub>AlC composites using Ti, Al and carbon nanotubes to attain a microstructure including equiaxed TiAl grains and interpenetrating networks of Ti<sub>2</sub>AlC. They reported that with increasing the SPS temperature from 950 to 1150 °C, the TiAl grains coarsened remarkably, which led to a drop in mechanical properties. Liu et al. [40] fabricated TiAl nanocomposites with fully lamellar microstructure and uniformly dispersed Ti<sub>2</sub>AlC precipitates by ball-milling and SPS of pre-alloyed Ti–48Al–2Nb–2Cr powder and graphene. They systematically discussed the relationship between the attained unique microstructure and outstanding oxidation resistance. Wang et al. [41] fabricated TiAl–Ti<sub>2</sub>AlN composites with an innovative network structure, i.e., distribution of the in-situ formed Ti<sub>2</sub>AlN around the fine lamellar TiAl matrix, by hot pressing route.

In the current research work, previously-synthesized Ti<sub>3</sub>AlC<sub>2</sub> additive with different amounts (10, 15, 20, 25, and 30 wt%) is added to in-situ synthesized TiAl intermetallic. Microstructure development during the SPS-manufactured TiAl–Ti<sub>3</sub>AlC<sub>2</sub> composites is reported as the 3<sup>rd</sup> part of a series of papers. The 1<sup>st</sup> and 2<sup>nd</sup> parts of this series were published recently and devoted to “sintering and densification” (Ref. [42]), and “phase evolution” (Ref. [43]), respectively. Mechanical and fractographical properties of the samples will be published in the near future.

## 2. Experimental procedure

MAX phase of Ti<sub>3</sub>AlC<sub>2</sub> was already synthesized in our laboratory at the Materials and Energy Research Center (MERC) via the self-propagating high-temperature synthesis (SHS) of the mechanically-activated elemental powder mixture of Ti, Al, and graphite (see details in Ref. [44]). It should be noted that the purity of produced MAX phase was 85 wt%, and in other words, 15 wt% TiC impurity was synthesized with it. The synthesized material was used in different amounts (10, 15, 20, 25, and 30 wt%) as the reinforcement phase in the TiAl matrix composites.

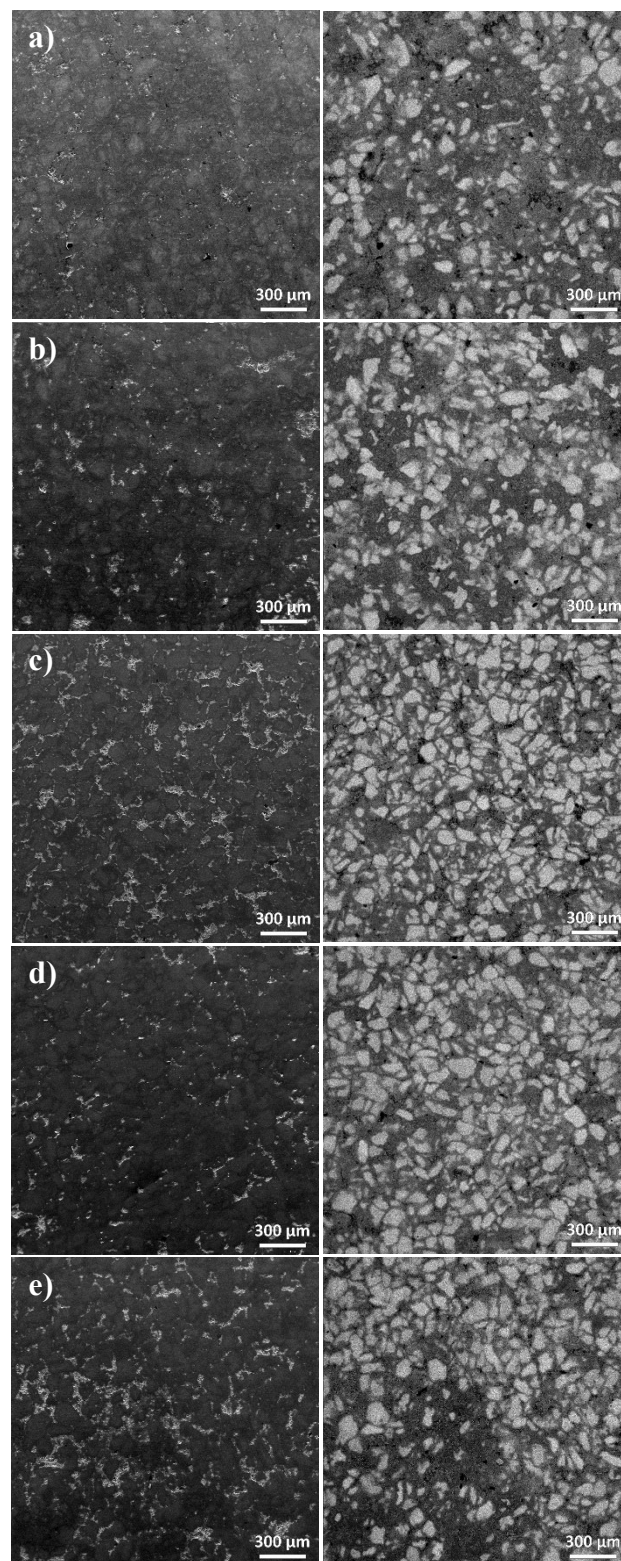


**Fig. 1.** SEM images of the polished surfaces of a) TiAl–10 wt% Ti<sub>3</sub>AlC<sub>2</sub>, b) TiAl–15 wt% Ti<sub>3</sub>AlC<sub>2</sub>, c) TiAl–20 wt% Ti<sub>3</sub>AlC<sub>2</sub>, d) TiAl–25 wt% Ti<sub>3</sub>AlC<sub>2</sub>, and e) TiAl–30 wt% Ti<sub>3</sub>AlC<sub>2</sub> composites.

Similar powders of Al and Ti, with equal molar ratios, were also employed as raw materials for in-situ manufacturing of TiAl matrix through spark plasma sintering process. Before performing the SPS

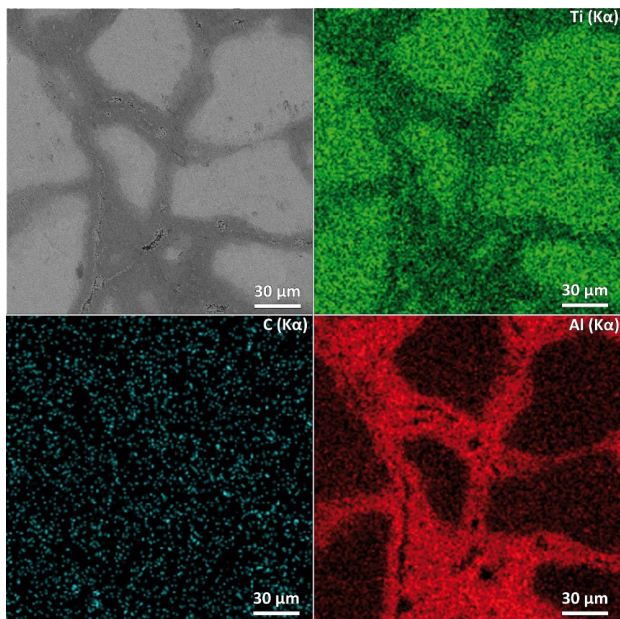


**Fig. 2.** SEM image of the polished surface and EDS elemental maps of TiAl–15 wt%  $\text{Ti}_3\text{AlC}_2$  composite.

process, Al, Ti and  $\text{Ti}_3\text{AlC}_2$  mixtures were mixed by 300 rpm ball-milling for 60 min. Subsequently, each mixture was separately poured into a suitable graphite mold, the prepared mold was placed in the SPS furnace (model: 20T-10), an initial vacuum of 12–15 Pa was supplied, and a preliminary pressure of  $\sim 8$  MPa was applied (see details in Ref. [42]). Finally, the synthesis and sintering processes were completed under 40 MPa load at 900 °C temperature for 7 min soaking time.

After grinding and cleaning the graphite foils attached to the sintered samples, sandpapers and diamond paste were used for final polishing. The prepared surfaces were microstructurally investigated by scanning electron microscopy (SEM: FEI ESEM Quanta200) and tested for chemical analysis (point, line scan and two-dimensional elemental map) with energy-dispersive X-ray spectroscopy (EDS: EDAX TEAM™).

### 3. Results and discussion

In this section, the microstructural results of TiAl– $\text{Ti}_3\text{AlC}_2$  composites are discussed, which is the 3<sup>rd</sup> part of a series of papers, two parts of which have already been published. In other words, for a more detailed study of the densification behavior and measured relative density values (reported in the 1<sup>st</sup> part of this series: Ref. [42]), and the in-situ phases formed during the synthesis and sintering processes (published as the 2<sup>nd</sup> part of this series: Ref. [43]), the microstructure development of TiAl– $\text{Ti}_3\text{AlC}_2$  composites is examined using SEM/EDS analyses.

SEM results captured from all five samples are presented in Fig. 1 (secondary and backscattered electron images on the left and right, respectively). In these images, two areas of light gray and dark gray can be seen. According to the EDS analysis performed on the samples, will be discussed below, it was found that the light gray phases are related to MAX phases and the dark gray phases are linked to titanium aluminides (TiAl and  $\text{Ti}_3\text{Al}$ ). Therefore, the developed microstructures are consistent with the XRD results. Yeh and Su [45] also detected the

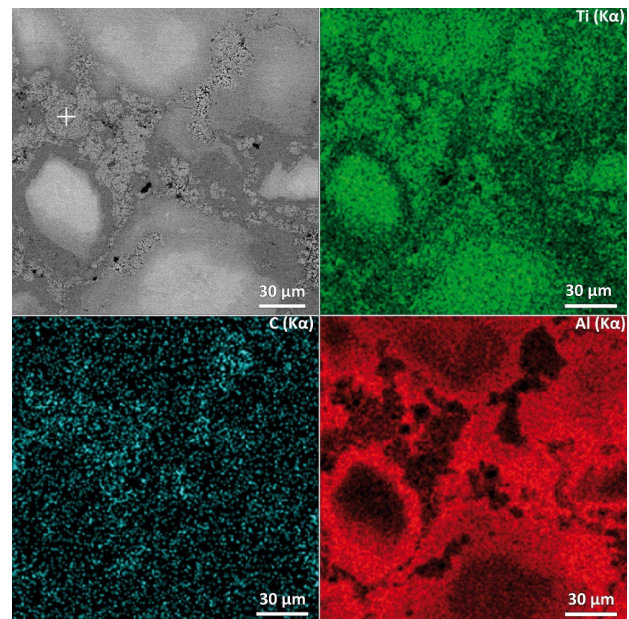


**Fig. 3.** SEM image of the polished surface and EDS elemental maps of TiAl–25 wt%  $\text{Ti}_3\text{AlC}_2$  composite.

$\text{Ti}_3\text{Al}$  intermetallic as a major secondary phase together with the TiAl due to the Ti–Al reaction during the self-propagating high-temperature synthesis (SHS) of elemental powders. Of course, it should be noted that light elements such as carbon are not accurately identifiable by EDS analysis and there are some errors in the quantitative evaluations. However, the results reported in the literature [46, 47] confirm the EDS outcomes of this study.

SEM images with higher magnification along with EDS elemental maps taken from two TiAl-based composites with 15 wt% and 25 wt%  $\text{Ti}_3\text{AlC}_2$  additives are presented in Figs. 2 and 3, respectively. The results of these figures also confirm the findings of the XRD analyses, as described in Ref. [43], so that TiAl,  $\text{Ti}_3\text{Al}$ ,  $\text{Ti}_3\text{AlC}_2$  and  $\text{Ti}_2\text{AlC}$  phases are detected in the sintered composites. The results of the quantitative analysis reported in Ref. [43] confirmed that although the

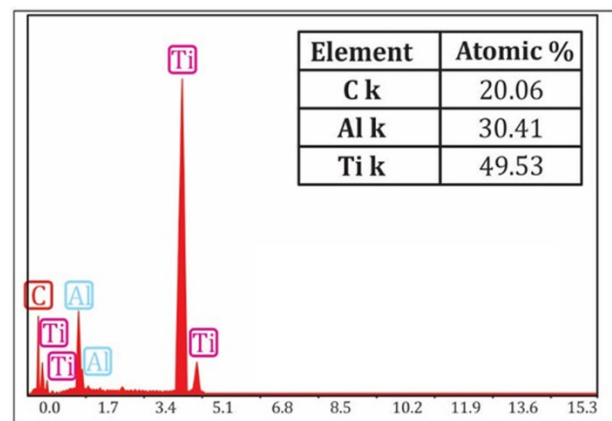


**Fig. 4.** EDS analysis taken from the point indicated by “+” in the SEM image of Fig. 3.

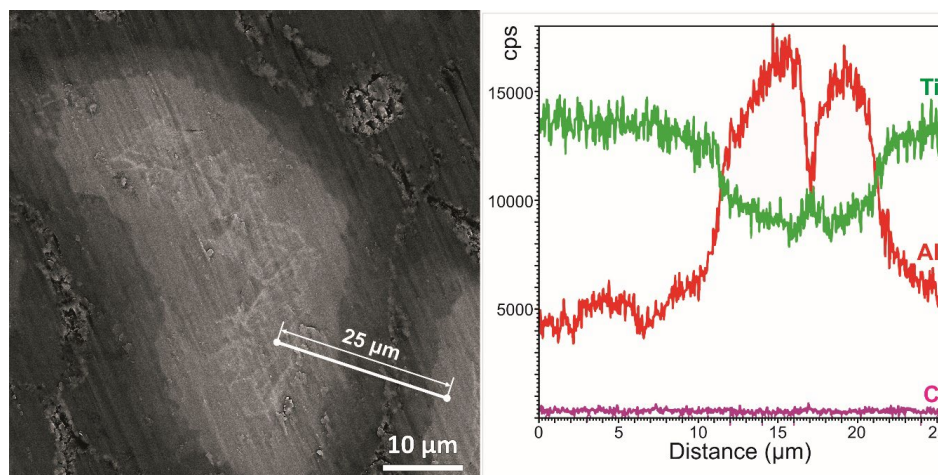


**Fig. 5.** SEM image of the polished surface and EDS line scan profiles of TiAl–20 wt% Ti<sub>3</sub>AlC<sub>2</sub> composite.

TiAl is the main phase of matrix, significant amounts of Ti<sub>3</sub>Al also appeared during the synthesis of the TiAl. Therefore, the matrix of composites prepared by SPS can be considered as a mixture of intermetallic compounds of TiAl (dominant phase) and Ti<sub>3</sub>Al. However, in the sample containing 25 wt% Ti<sub>3</sub>AlC<sub>2</sub>, due to the more contact of the TiAl matrix with the MAX phase additive, the reaction of TiC particles (synthesized as impurity along with the Ti<sub>3</sub>AlC<sub>2</sub> reinforcement) with the matrix phase is more probable. As a result, the amount of SPS-induced Ti<sub>2</sub>AlC phase is higher. Chen et al. [38] found that during the hot pressing of Ti/Al/C and Ti/Al/TiC powder mixtures, aimed at making TiAl–Ti<sub>2</sub>AlC composites, titanium reacts with aluminum to form TiAl below 900 °C, but above this temperature, TiAl reacts with TiC to form fine grain TiAl–Ti<sub>2</sub>AlC microstructure with homogeneous distribution of Ti<sub>2</sub>AlC MAX phase in TiAl matrix.

Fig. 4 shows the results of EDS analysis taken from the in-situ synthesized Ti<sub>2</sub>AlC phase at the grain boundaries, indicated by “+” in the SEM image of Fig. 3. The measured atomic percentages (approximately 50, 30, and 20 at% for the titanium, aluminum and carbon, respectively) are compatible with the stoichiometric ratios of the elements in the Ti<sub>2</sub>AlC compound (50, 25, and 25% for the titanium, aluminum and carbon, respectively). The reason of the lower value measured by EDS analysis for the carbon may be related to the light nature of this element.

The high-magnification SEM image and EDS line scan analysis of the polished surface of the composite sample with 20 wt% Ti<sub>3</sub>AlC<sub>2</sub> additive are shown in Fig. 5. As can be seen, the light Ti<sub>3</sub>AlC<sub>2</sub> MAX phases are seen along with the dark titanium aluminide matrix. This observation is well consistent with the results obtained from EDS line scan profiles. Based on this figure, it is clear that Ti with a green profile has a lower concentration in the dark phases than in the light ones. This observation is consistent with the assumption that the dark and light regions correspond to the titanium aluminide and Ti<sub>3</sub>AlC<sub>2</sub> phases, respectively, because given the chemical formula of the two compounds, it is obvious that the atomic percentage of Ti in the Ti<sub>3</sub>AlC<sub>2</sub> MAX phase is three times greater than the atomic percentage of Al. However, these two elements have equal atomic percentages in the composition of TiAl intermetallic. A similar trend can be seen in the red profile of Al, which has an inverse behavior of Ti concentration variations.

The Ti<sub>2</sub>AlC MAX phase, which is synthesized at the grain boundaries of the TiAl matrix, is also seen in this micrograph. Elemental analysis of this phase (Ti<sub>2</sub>AlC), which corresponds to the distance of ~17 μm in the horizontal axis of the EDS line scan analysis, indicates that the Ti<sub>2</sub>AlC has more titanium than the TiAl but less titanium than the Ti<sub>3</sub>AlC<sub>2</sub>. Also, the concentration of aluminum in Ti<sub>2</sub>AlC is less than TiAl phase but higher than Ti<sub>3</sub>AlC<sub>2</sub>. Both observations are perfectly consistent with the stoichiometric ratios of Al and Ti elements in the chemical formulas of these three compounds. Another interesting point is that although carbon is a light element and the result of EDS analysis is not much reliable, in the purple profile of C, a slight peak is seen at the distance of 17 μm. This observation is also in harmony with the presence of carbon in the Ti<sub>2</sub>AlC but its absence in the TiAl.

#### 4. Conclusions

In the 3<sup>rd</sup> part of a series of publications, devoted to processing-microstructure-properties correlations in TiAl–Ti<sub>3</sub>AlC<sub>2</sub> composites, the microstructural development during the synthesis/sintering of starting Ti<sub>3</sub>AlC<sub>2</sub> (10, 15, 20, 25, and 30 wt%) as well as Ti and Al materials was investigated. Along with the ex-situ added Ti<sub>3</sub>AlC<sub>2</sub> MAX phase, the in-situ formed TiAl/Ti<sub>3</sub>Al intermetallics and another MAX phase (Ti<sub>2</sub>AlC) were seen in the sintered microstructures created by SPS at 900 °C. The Ti<sub>2</sub>AlC was in-situ synthesized through the chemical reaction between TiC impurity and part of the TiAl. All of the above-mentioned observations, revealed by SEM along with EDS via the point, line scan and two-dimensional map analyses, were in complete agreement with the findings of densification and phase analysis performed in the 1<sup>st</sup> and 2<sup>nd</sup> parts of this research study.

#### CRedit authorship contribution statement

**Maryam Akhlaghi:** Investigation, Data curation, Writing – original draft, Visualization.

**Esmail Salahi:** Project administration, Supervision, Methodology.

**Seyed Ali Tayebifard:** Conceptualization, Funding acquisition, Validation.

**Gert Schmidt:** Writing – review & editing.

## Data availability

The data underlying this article will be shared on reasonable request to the corresponding author.

## Declaration of competing interest

The authors declare no competing interests.

## Funding and acknowledgment

The content of this article is based on the PhD thesis of the first author. The authors would like to express their gratitude to the Materials and Energy Research Center for its support of this research project under grant number 481394051. Additionally, the invaluable assistance of Dr. Behzad Nayeibi in result analysis and Mrs. Masoumeh Enayati and Mrs. Nadi Shojaei in conducting the experiments is sincerely appreciated.

## References

- [1] Y. Pan, X. Lu, C. Liu, T. Hui, C. Zhang, X. Qu, Sintering densification, microstructure and mechanical properties of Sn-doped high Nb-containing TiAl alloys fabricated by pressureless sintering, *Intermetallics*. 125 (2020) 106891. <https://doi.org/10.1016/j.intermet.2020.106891>.
- [2] M. Yan, F. Yang, B. Lu, C. Chen, Y. Sui, Z. Guo, Microstructure and mechanical properties of high relative density  $\gamma$ -TiAl alloy using irregular pre-alloyed powder, *Metals (Basel)*. 11 (2021) 635. <https://doi.org/10.3390/met11040635>.
- [3] D. Martins, F. Grumbach, A. Simoulin, P. Sallot, K. Mocellin, et al., Spark plasma sintering of a commercial TiAl 48-2-2 powder: Densification and creep analysis, *Mater. Sci. Eng. A*. 711 (2018) 313–316. <https://doi.org/10.1016/j.msea.2017.11.041>.
- [4] M. Musi, B. Galy, J.-P. Monchoux, A. Couret, H. Clemens, S. Mayer, In-situ observation of the phase evolution during an electromagnetic-assisted sintering experiment of an intermetallic  $\gamma$ -TiAl based alloy, *Scr. Mater.* 206 (2022) 114233. <https://doi.org/10.1016/j.scriptamat.2021.114233>.
- [5] A. Couret, G. Molénat, J. Galy, M. Thomas, Microstructures and mechanical properties of TiAl alloys consolidated by spark plasma sintering, *Intermetallics*. 16 (2008) 1134–1141. <https://doi.org/10.1016/j.intermet.2008.06.015>.
- [6] D. Wimler, J. Lindemann, H. Clemens, S. Mayer, Microstructural evolution and mechanical properties of an advanced  $\gamma$ -TiAl based alloy processed by spark plasma sintering, *Materials (Basel)*. 12 (2019) 1523. <https://doi.org/10.3390/ma12091523>.
- [7] A. Mohammadnejad, A. Bahrami, L. Tafaghodi Khajavi, Microstructure and mechanical properties of spark plasma sintered nanocrystalline TiAl-xB composites ( $0.0 < x < 1.5$  at.%) containing carbon nanotubes, *J. Mater. Eng. Perform.* 30 (2021) 4380–4392. <https://doi.org/10.1007/s11665-021-05773-6>.
- [8] X. Liu, Q. Lin, W. Zhang, C. Van Horne, L. Cha, Microstructure design and its effect on mechanical properties in gamma titanium aluminides, *Metals (Basel)*. 11 (2021) 1644. <https://doi.org/10.3390/met11101644>.
- [9] L. Wang, Y. Zhang, X. Hua, C. Shen, F. Li, et al., Fabrication of  $\gamma$ -TiAl intermetallic alloy using the twin-wire plasma arc additive manufacturing process: Microstructure evolution and mechanical properties, *Mater. Sci. Eng. A*. 812 (2021) 141056. <https://doi.org/10.1016/j.msea.2021.141056>.
- [10] M. Shahedi Asl, B. Nayeibi, M. Farvizi, R. Alaghmandfard, M. Shokouhimehr, et al., Formation of Al–Al<sub>2</sub>O<sub>3</sub> core–shell nanosphere chains during electron beam melting of  $\gamma$ -TiAl, *Intermetallics*. 136 (2021) 107261. <https://doi.org/10.1016/j.intermet.2021.107261>.
- [11] A. Couret, M. Allen, M.W. Rackel, B. Galy, J.-P. Monchoux, et al., Chemical heterogeneities in tungsten containing TiAl alloys processed by powder metallurgy, *Materialia*. 18 (2021) 101147. <https://doi.org/10.1016/j.mtla.2021.101147>.
- [12] C. Zhang, Y. Pan, T. Hui, W. Xu, S. Zhang, et al., The sintering densification, microstructure and mechanical properties of Ti–48Al–2Cr–2Nb by a small addition of Sn–Al powder, *J. Mater. Res. Technol.* 15 (2021) 6947–6955. <https://doi.org/10.1016/j.jmrt.2021.11.096>.
- [13] F. Wenbin, H. Lianxi, H. Wenxiong, W. Erde, L. Xiaoping, Microstructure and properties of a TiAl alloy prepared by mechanical milling and subsequent reactive sintering, *Mater. Sci. Eng. A*. 403 (2005) 186–190. <https://doi.org/10.1016/j.msea.2005.04.049>.
- [14] S. Xiao, J. Tian, L. Xu, Y. Chen, H. Yu, J. Han, Microstructures and mechanical properties of TiAl alloy prepared by spark plasma sintering, *Trans. Nonferrous Met. Soc. China*. 19 (2009) 1423–1427. [https://doi.org/10.1016/S1003-6326\(09\)60044-3](https://doi.org/10.1016/S1003-6326(09)60044-3).
- [15] Y.A. Kozhakhmetov, M.K. Skakov, S.R. Kurbanbekov, N.M. Mukhamedov, N.Y. Mukhamedov, Powder composition structuration of the Ti-25Al-25Nb (at.%) system upon mechanical activation and subsequent spark plasma sintering, *Eurasian Chem.-Technol. J.* 23 (2021) 37. <https://doi.org/10.18321/ectj1032>.
- [16] M. Akhlaghi, S.A. Tayebifard, E. Salahi, M. Shahedi Asl, Spark plasma sintering of TiAl–Ti<sub>3</sub>AlC<sub>2</sub> composite, *Ceram. Int.* 44 (2018) 21759–21764. <https://doi.org/10.1016/j.ceramint.2018.08.272>.
- [17] H. Jabbar, A. Couret, L. Durand, J.-P. Monchoux, Identification of microstructural mechanisms during densification of a TiAl alloy by spark plasma sintering, *J. Alloys Compd.* 509 (2011) 9826–9835. <https://doi.org/10.1016/j.jallcom.2011.08.008>.
- [18] N.F. Mogale, W.R. Matizamhuka, Spark plasma sintering of titanium aluminides: a progress review on processing, structure-property relations, alloy development and challenges, *Metals (Basel)*. 10 (2020) 1080. <https://doi.org/10.3390/met10081080>.
- [19] Y. Kozhakhmetov, M. Skakov, N. Mukhamedova, S. Kurbanbekov, S. Ramankulov, W. Wieleba, Changes in the microstructural state of Ti-Al-Nb-based alloys depending on the temperature cycle during spark plasma sintering, *Mater. Test.* 63 (2021) 119–123. <https://doi.org/10.1515/mt-2020-0017>.
- [20] Z.M. Sun, Q. Wang, H. Hashimoto, S. Tada, T. Abe, Synthesis and consolidation of TiAl by MA–PDS process from sponge-Ti and chip-Al, *Intermetallics*. 11 (2003) 63–69. [https://doi.org/10.1016/S0966-9795\(02\)00183-8](https://doi.org/10.1016/S0966-9795(02)00183-8).
- [21] D. Wimler, J. Lindemann, T. Kremmer, H. Clemens, S. Mayer, Microstructure and mechanical properties of novel TiAl alloys tailored via phase and precipitate morphology, *Intermetallics*. 138 (2021) 107316. <https://doi.org/10.1016/j.intermet.2021.107316>.
- [22] M. Cabibbo, A. Knaislová, P. Novák, F. Průša, C. Paoletti, Role of Si on lamellar formation and mechanical response of two SPS Ti–15Al–15Si and Ti–10Al–20Si intermetallic alloys, *Intermetallics*. 131 (2021) 107099. <https://doi.org/10.1016/j.intermet.2021.107099>.
- [23] B.-A. Behrens, K. Brunotte, J. Peddinghaus, A. Heymann, Influence of dwell time and pressure on SPS process with titanium aluminides, *Metals (Basel)*. 12 (2022) 83. <https://doi.org/10.3390/met12010083>.
- [24] Y. Su, Y. Lin, N. Zhang, D. Zhang, Microstructures and mechanical properties of TiAl alloy fabricated by spark plasma sintering, *Int. J. Mod. Phys. B*. 34 (2020) 2040036. <https://doi.org/10.1142/S0217979220400366>.
- [25] H. Jabbar, J.-P. Monchoux, F. Houdellier, M. Dollé, F.-P. Schimansky, et al., Microstructure and mechanical properties of high niobium containing TiAl alloys elaborated by spark plasma sintering, *Intermetallics*. 18 (2010) 2312–2321. <https://doi.org/10.1016/j.intermet.2010.07.024>.
- [26] X. Gu, F. Cao, N. Liu, G. Zhang, D. Yang, et al., Microstructural evolution and mechanical properties of a high yttrium containing TiAl based alloy densified by spark plasma sintering, *J. Alloys*

- Compd. 819 (2020) 153264.  
<https://doi.org/10.1016/j.jallcom.2019.153264>.
- [27] Y.Y. Chen, H.B. Yu, D.L. Zhang, L.H. Chai, Effect of spark plasma sintering temperature on microstructure and mechanical properties of an ultrafine grained TiAl intermetallic alloy, *Mater. Sci. Eng. A*. 525 (2009) 166–173. <https://doi.org/10.1016/j.msea.2009.06.056>.
- [28] T. Voisin, J.-P. Monchoux, M. Hantcherli, S. Mayer, H. Clemens, A. Couret, Microstructures and mechanical properties of a multi-phase  $\beta$ -solidifying TiAl alloy densified by spark plasma sintering, *Acta Mater.* 73 (2014) 107–115.  
<https://doi.org/10.1016/j.actamat.2014.03.058>.
- [29] Y.H. Wang, J.P. Lin, Y.H. He, Y.L. Wang, G.L. Chen, Fabrication and SPS microstructures of Ti–45Al–8.5Nb–(W,B,Y) alloying powders, *Intermetallics*. 16 (2008) 215–224.  
<https://doi.org/10.1016/j.intermet.2007.09.010>.
- [30] D. Zhu, L. Liu, D. Dong, X. Wang, Y. Liu, et al., Microstructure and compression behavior of in-situ synthesized Ti<sub>2</sub>AlC reinforced Ti–48Al–2Cr alloy with carbon nanotubes addition, *J. Alloys Compd.* 862 (2021) 158646. <https://doi.org/10.1016/j.jallcom.2021.158646>.
- [31] F. Zakeri Shahroudi, B. Ghasemi, H. Abdolapour, M. Razavi, Sintering behavior of Cr<sub>2</sub>AlC MAX phase synthesized by Spark plasma sintering, *Int. J. Appl. Ceram. Technol.* 19 (2022) 1309–1318.  
<https://doi.org/10.1111/ijac.13995>.
- [32] S. Haji Amiri, M. Ghassemi Kakroudi, N. Pourmohammadi Vafa, M. Shahedi Asl, Synthesis and sintering of Ti<sub>3</sub>SiC<sub>2</sub>–SiC composites through reactive hot-pressing of TiC and Si precursors, *Silicon*. 14 (2021) 4227–4235. <https://doi.org/10.1007/s12633-021-01207-z>.
- [33] S. Haji Amiri, N. Pourmohammadi Vafa, Microstructure and mechanical properties of Ti<sub>3</sub>SiC<sub>2</sub> MAX phases sintered by hot pressing, *Synth. Sinter.* 1 (2021) 216–222.  
<https://doi.org/10.53063/synsint.2021.1472>.
- [34] E. Gholami nejad, M. Farvizi, A. Habibolahzadeh, Microstructure and tribological behavior of Ti<sub>2</sub>AlN MAX phase synthesized through mechanical activation–spark plasma sintering method, *J. Mater. Eng. Perform.* 31 (2022) 5050–5062.  
<https://doi.org/10.1007/s11665-021-06559-6>.
- [35] J. Lyu, E.B. Kashkarov, N. Travitzky, M.S. Syrtanov, A.M. Lider, Sintering of MAX-phase materials by spark plasma and other methods, *J. Mater. Sci.* 56 (2021) 1980–2015.  
<https://doi.org/10.1007/s10853-020-05359-y>.
- [36] S. Haji Amiri, M. Ghassemi Kakroudi, T. Rabizadeh, M. Shahedi Asl, Characterization of hot-pressed Ti<sub>3</sub>SiC<sub>2</sub>–SiC composites, *Int. J. Refract. Met. Hard Mater.* 90 (2020) 105232.  
<https://doi.org/10.1016/j.jrmhm.2020.105232>.
- [37] B. Mei, Y. Miyamoto, Investigation of TiAl/Ti<sub>2</sub>AlC composites prepared by spark plasma sintering, *Mater. Chem. Phys.* 75 (2002) 291–295. [https://doi.org/10.1016/S0254-0584\(02\)00078-0](https://doi.org/10.1016/S0254-0584(02)00078-0).
- [38] Y.-L. Chen, M. Yan, Y.-M. Sun, B.-C. Mei, J.-Q. Zhu, The phase transformation and microstructure of TiAl/Ti<sub>2</sub>AlC composites caused by hot pressing, *Ceram. Int.* 35 (2009) 1807–1812.  
<https://doi.org/10.1016/j.ceramint.2008.10.009>.
- [39] F. Yang, F.T. Kong, Y.Y. Chen, S.L. Xiao, Effect of spark plasma sintering temperature on the microstructure and mechanical properties of a Ti<sub>2</sub>AlC/TiAl composite, *J. Alloys Compd.* 496 (2010) 462–466. <https://doi.org/10.1016/j.jallcom.2010.02.077>.
- [40] C. Liu, Y. Wang, W. Han, T. Ma, D. Ma, Y. Zhang, Achieving superior high-temperature strength and oxidation resistance of TiAl nanocomposite through in situ semicoherent MAX phase precipitation, *ACS Appl. Mater. Interfaces*. 14 (2022) 8394–8403.  
<https://doi.org/10.1021/acsami.1c21719>.
- [41] D. Wang, D. Sun, X. Han, Q. Wang, In situ Ti<sub>2</sub>AlN reinforced TiAl-based composite with a novel network structure: Microstructure and flexural property at elevated temperatures, *Mater. Sci. Eng. A*. 742 (2019) 231–240. <https://doi.org/10.1016/j.msea.2018.11.018>.
- [42] M. Akhlaghi, E. Salahi, S.A. Tayebifard, G. Schmidt, Role of Ti<sub>3</sub>AlC<sub>2</sub> MAX phase on characteristics of in-situ synthesized TiAl intermetallics. Part I: sintering and densification, *Synth. Sinter.* 1 (2021) 169–175. <https://doi.org/10.53063/synsint.2021.1347>.
- [43] M. Akhlaghi, E. Salahi, S.A. Tayebifard, G. Schmidt, Role of Ti<sub>3</sub>AlC<sub>2</sub> MAX phase on characteristics of in-situ synthesized TiAl intermetallics. Part II: Phase evolution, *Synth. Sinter.* 1 (2021) 211–216. <https://doi.org/10.53063/synsint.2021.1453>.
- [44] M. Akhlaghi, S.A. Tayebifard, E. Salahi, M. Shahedi Asl, G. Schmidt, Self-propagating high-temperature synthesis of Ti<sub>3</sub>AlC<sub>2</sub> MAX phase from mechanically-activated Ti/Al/graphite powder mixture, *Ceram. Int.* 44 (2018) 9671–9678.  
<https://doi.org/10.1016/j.ceramint.2018.02.195>.
- [45] C.L. Yeh, S.H. Su, In situ formation of TiAl–TiB<sub>2</sub> composite by SHS, *J. Alloys Compd.* 407 (2006) 150–156.  
<https://doi.org/10.1016/j.jallcom.2005.06.053>.
- [46] R. Orrú, G. Cao, Z.A. Munir, Field-activated combustion synthesis of titanium aluminides, *Metall. Mater. Trans. A*. 30 (1999) 1101–1108. <https://doi.org/10.1007/s11661-999-0162-1>.
- [47] T.T. Ai, Microstructures and mechanical properties of in-situ Al<sub>2</sub>O<sub>3</sub>/TiAl composites by exothermic dispersion method, *Acta Metall. Sin. (Engl. Lett.)*. 21 (2008) 437–443.  
[https://doi.org/10.1016/S1006-7191\(09\)60006-5](https://doi.org/10.1016/S1006-7191(09)60006-5).